Proceedings of the Pakistan Academy of Sciences: A Physical and Computational Sciences 61(3): 293-302 (2024)
Copyright © Pakistan Academy of Sciences
ISSN (Print): 2518-4245; ISSN (Online): 2518-4253
http://doi.org/10.53560/PPASA(61-3)866

Pakistan Academy of Sciences

Research Article

Numerical Study on Failure Mechanism of Rock Slope Formed by Mudstone at Girdu, Pakistan

Zulkifl Ahmed[1], Sumra Yousuf[2*], Muhammad Rizwan[3], Muhammad Yousaf Raza Taseer[2], Muhammad Qasim Sultan[1], Mahwish Zahra[4], and Anum Aleha[4]

[1]Department of Civil Technology, Mir Chakar Khan Rind University of Technology, DG Khan, Pakistan

[2] Department of Building and Architectural Engineering, Faculty of Engineering and Technology, Bahauddin Zakariya University, Multan, Pakistan

[3]Department of Metallurgical Engineering, NED University of Engineering and Technology, Karachi, Pakistan

[4]Department of Architecture Design, National Fertilizer Corporation Institute of Engineering and Technology, Multan, Pakistan

Abstract: Failure analysis of rock slope is a core topic in rock mechanics and geotechnical engineering. This paper simulates the failure mechanism of a rock slope formed by mudstone at Girdu, Pakistan. Initially, site surveys and laboratory experiments were carried out to measure slope geometry and input shear strength properties of the material. The geotechnical structure and model analyzing computer program (GeoSMA^{3D}) was used to determine the stability of the main slippery blocks. A shear strength reduction method was selected in a three-dimensional distinct element code (3DEC) to examine the failure mechanism, the factor of safety (*FS*), shear strain concentration, and displacement of slope at various monitoring points. Furthermore, the effect of the rock slippery block, slope angle, and slope height on failure modes of slope were assessed. The present results showed that the studied section is prone to big planer failure at both maximum and minimum strength properties. Slope angle and height significantly influenced the failure characteristics of rock slope . It is inferred that these parameters must be precisely considered during slope reinforcement design.

Keywords: Rock Slope, Stability Analysis, Factor of Safety, GeoSMA^{3D}, 3DEC.

1. INTRODUCTION

Landslides are one of the most common geological natural hazards. Every year, many disastrous landslides occur all over the world, causing loss of property and life [1, 2]. This causes significant fatalities, economic losses injuries, and property damages. In the past decades, many methodologies have been proposed to reduce the risk of harm caused by rock failure. For highway planners slope failure hazards are the major concern for vehicle transportation and economic opinion [3, 4]. Slope failure mechanisms mostly depend on material strength, geological conditions, climatic conditions, hydrological conditions, slope geometry, and discontinuity characterization [5, 6]. Slope failure includes lateral spread, erosion, toppling, wedge sliding, creep, rotational landslides, tension cracking, translational landslides, squeezing, rock-fall, and sliding after loss of toe support [7].

Slope failure is a type of shear failure that causes detachment of unsupported rock material. Sometimes, rock failure can be naturally under the influence of gravity, like freeze-thaw cycles slide [8], or seismic exertion [9]. Therefore, the motion

Received: June 2024; Revised: August 2024; Accepted: September 2024
* Corresponding Author: Sumra Yousuf <sumra.yousafrm@gmail.com>

of rock fall is mostly dependent on the volume of the sliding surface, its geometry, the shape of the sliding blocks, slope inclination angle, and surface irregularities [10]. Sometimes slope failure occurs due to the effect of heavy machine movement and blasting [11]. However, the displacement of rounded-shaped blocks was more than compared to square-shaped blocks [12]. The height of the slope, its dip angle, and the volume of the sliding surface categorize the motions of the rock slope. In previous studies, four types of rock motion have been discussed, such as sliding, bouncing, free fall, and rolling [13]. The simulation of the rock failure mechanism is a complex process that plays an important role in understanding rock-fall hazards. During rock slope stability analysis, estimating safety factors is a difficult and important task. For this purpose, a great effort has been made to develop a suitable computer code that can directly and efficiently simulate slope stability factor and displacement. In previous studies, Wang *et al*. [14] established GeoSMA^{3D} software to judge the stability of rock blocks. Liu *et al*. [15] applied the UDEC simulator to study the effect of blasting on jointed rock slopes. Sarkar *et al*. [16] assessed slope stability and landslide hazard by finite element analysis. Singh *et al*. [17] selected finite element computer code to simulate the stability of road-cut cliffs in basaltic rock mass. Zhao *et al*. [18] used unmanned aerial vehicle (UAV) photogrammetry to investigate the stability of rock cliff faces and multistep rock slopes. Kou *et al*. [19] used the article hydrodynamics method to study the progressive failure process of jointed rock slope. Gautam and Mehndiratta [20] applied FLAC^{2D} to analyze the rock slope stability considering an infilled planer. These studies computed the stability of rock considering joints ignoring key slippery blocks. Also, no one simulated the failure mechanism of rock slopes formed by mudstone.

In the present study, geotechnical structure and model analyzing (GeoSMA^{3D}) software was first applied to simulate the stability of rock slippery blocks. Then, 3DEC was used to simulate the stability of a rock slope formed by mudstone at station point 5 + 800, Girdu, Pakistan. Finally, the effect of several parameters on the slope failure profile was studied using 3DEC software.

2. STUDY AREA AND GEOLOGY

Girdu Hill Station is located in the Suleiman Mountains near Fort Munro, Pakistan. The Suleiman Mountains are a mountain range in Pakistan, located in the central part of the country as shown in Figure 1. These are the southern part of the Hindu Kush Mountains and extend into the Baluchistan, Khyber Pakhtunkhwa, and Punjab Provinces. The Girdu hilly area separates the Punjab province from the Baluchistan province. The eastern face of the Girdu hills dip steeply to the Indus River and its altitude is 1800 meters. The National Highway N70 transects the Girdu Hill Station, making it a pivotal route for travelers and goods transport. It is 85 (Km) away toward the west of the City. The National Highway N70 connects the Punjab province to the Baluchistan province. The geological formation of the rock is mudstone. Physical analysis of rock slope shows three dominant discontinuity sets J_1, J_2 and J_3 dipping at different angles, as shown in Figure 2. Discontinuity sets have incessant lengths in the range of several meters. The discontinuity J_1 dips towards the road and J_1, and J_2 dips in the direction of the hill. The orientation of the discontinuities was judged during the field investigation as presented in Table 1. The true dip and dip direction of discontinuity were measured by a geological compass. The height and the length of the slope are 20 (m) and 500 (m), respectively, which is measured with a total station.

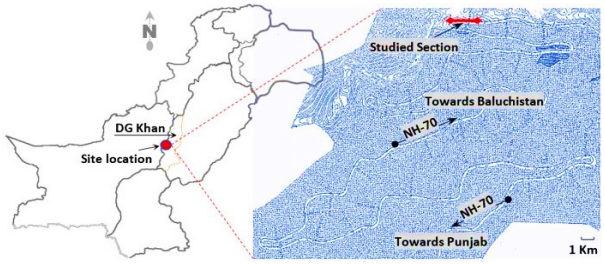

Fig. 1. Site location map (a) and Road alignment in red color (b).

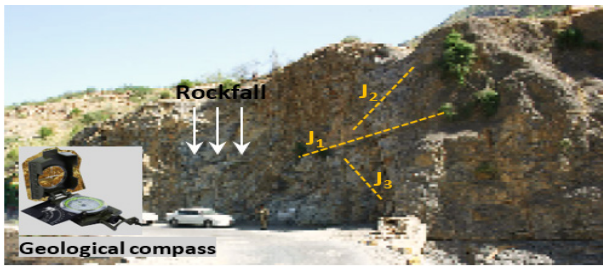

Fig. 2. Topographical, joint distribution, and rockfall at the station (5 + 800).

Table 1. Discontinuity orientation at the study area.

Discontinuity	True dip (°)	Dip direction (°)
JI	41-7	302-3
J2	66-2	279-9
J3	91-1	173-4
Flaws	13-5	069-2

3. METHODOLOGY

3.1. Laboratory Experiments

A uniaxial test is performed to estimate the mechanical properties of mudstone at various axial stresses (σ). Figure 3 shows the mudstone's results and deformation modes. Density, cohesion (*c*), and internal friction (ϕ) were determined by the uniaxial test (Table 2). The normal and shear stiffness of joints were estimated from the rock mass modulus, intact rock modulus, and joint spacing, assuming that the deformability of rock layers is due to the deformability of the intact rock and the deformability of the joints.

3.2. Identification of Slippery Blocks

During the field survey, two types of failure surfaces of the slippery blocks were noticed (Figure 4). The first type was formed due to the intersection of the slope surface with the slope shoulder, and the other type was formed by the slope face and discontinuity intersection. The dip angles of these surfaces are θ_1 and θ_2, respectively. The coordinates of the slope shoulder are (x_1, y_1, z_1) and (x_2, y_2, z_2). Several blocks are formed on the slope face due to the presence of joints. The presence of the rock blocks on the face of a slope increases the instability resulting in slope failure [20]. Joint surfaces were traversed with the slope shoulder. The slope coordinates are governed by the following Equation (1).

$$\frac{x - x_1}{x_2 - x_1} = \frac{y - y_1}{y_2 - y_1} = \frac{z - z_1}{z_2 - z_1} \quad (1)$$

The radius of the slope is *r*, the center of coordinates is x_0, y_0, z_0 and the dip direction is α. So, with the help of a normal vector (*l, m, n*) the equation of the joint plane can be expressed in Equation (2) as:

$$l(x - x_0) + m(y - y_0) + n(z - z_0) = 0 \quad (2)$$

Equation (3) will be tested if there is a factual resolution from Equations (1) and (2) as:

$$\begin{cases} x_1 \le x \le x_2 \\ y_1 \le y \le y_2 \\ z_1 \le z \le z_2 \\ (x - x_0)^2 + (y - y_0)^2 + (z - z_0)^2 \le r^2 \end{cases} \quad (3)$$

If the attained factual result satisfies Equation (3), this means that the slope shoulder and joint plane intersect with each other. So, both Equations (4) and (5) can be applied to judge the joint plane *i* and *j* respectively, as:

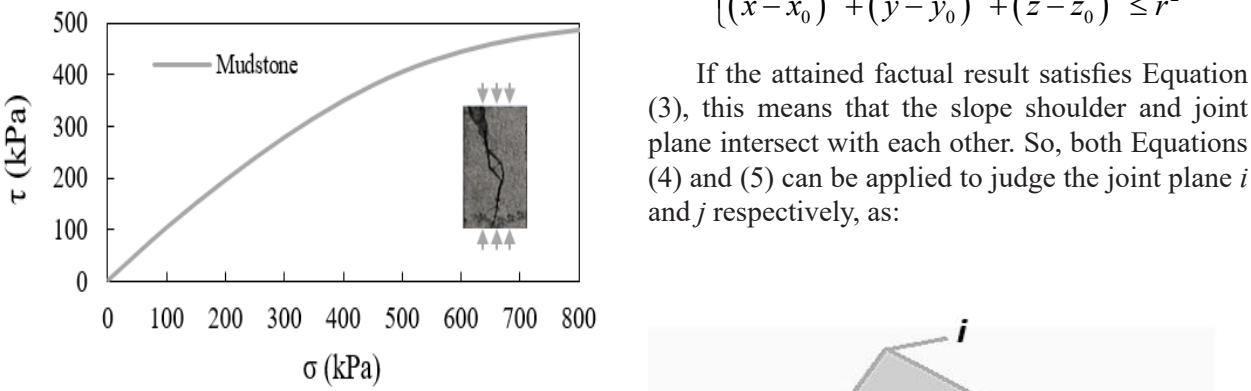

Fig. 3. Experimental results and deformation of mudstone sample.

Table 2. Mechanical properties of cut slope material maximum and minimum values.

Material	Density (g/cm³)	c (MPa)	ϕ (°)	Kn (GPa/m)	Ks (GPa/m)
Rock	2.03	3.54	32	25.27	6.1
Mudstone	1.61	0.08	22.9	22.67	5.73

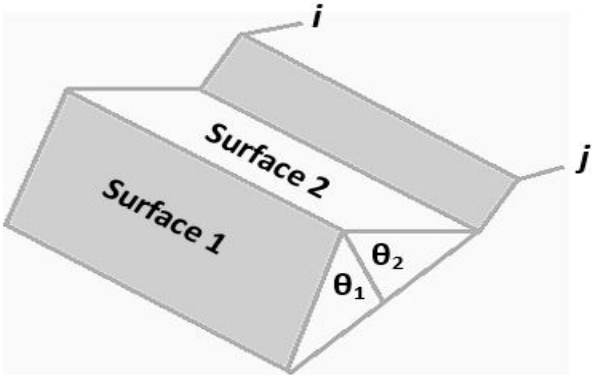

Fig. 4. Sliding model showing the failure mechanism for double failure surface.

$$Aix + Biy + Ciz + Di = 0 \quad (4)$$

$$Ajx + Bjy + Cjz + Dj = 0 \quad (5)$$

For the top of the cut slope, the plane equation is:

$$Ax + By + Cz + D = 0 \quad (6)$$

If $\Delta = \begin{vmatrix} Ai & Bi & Ci \\ Aj & Bj & Cj \\ A & B & C \end{vmatrix} = 0$, then Equations (4), (5), and (6) have no factual solutions, and discontinuity planes *i* and *j* seem on the crest of the cut slope. In contrast, the factual solution is explained as:

$$x = -\frac{\Delta x}{\Delta},\ y = -\frac{\Delta y}{\Delta},\ z = -\frac{\Delta z}{\Delta} \quad (7)$$

$$\Delta x = \begin{vmatrix} Di & Bi & Ci \\ Dj & Bj & Cj \\ D & B & C \end{vmatrix}\ \Delta y = \begin{vmatrix} Ai & Di & Ci \\ Aj & Dj & Cj \\ A & D & C \end{vmatrix} \text{ and } \Delta = \begin{vmatrix} Ai & Bi & Di \\ Aj & Bj & Dj \\ A & B & D \end{vmatrix} \quad (8)$$

Then, within the joint planes *i* and *j*, Equation (9) has been used to evaluate the corresponding joint planes.

$$\begin{cases} (xi - x)^2 + (yi - y)^2 + (zi - z)^2 \le ri^2 \\ (xj - x)^2 + (yj - y)^2 + (zj - z)^2 \le rj^2 \end{cases} \quad (9)$$

Where x_i, y_i, and z_i are coordinates, x_j, y_j, *and* z_j are midpoints of discontinuity planes, and r_i and r_j are the radii. Results can lead to the ultimate judgment of obtainable slippery blocks.

Equation (5) satisfies Equation (6) and Equation (7) based on discontinuity planes, coordinates, and radius of the failure surface. This solution leads to the final judgment of sliding surfaces, sliding blocks, and the corresponding radius of the slip circle of the slope [21].

3.3. Slippery Block Stability Calculation

After getting the coordinates, dip direction (α), and dip angle (β) of the sliding plane, the cosine of the inclination (θ) is calculated from the spatial geometry of the sliding surface. In the sliding mechanism, two sliding surfaces detached from the parent rock at the same time, when the coordinates of two points *A* and *C* are (x_a, y_a, z_a) and (x_c, y_c, z_c), respectively. The angle between the two surfaces was θ_1 and θ_2, which satisfies Equation (8). So, the *FS* of the double sliding model can be elaborated as Equation (9). The energy equation of the model can be shown as Equation (10).

$$\cos\theta = \frac{n}{\sqrt{l^2+m^2+n^2}} \quad (10)$$

Where $l = \sin\alpha\sin\beta, m = \sin\alpha\cos\beta, n = \cos\alpha$, β is the dip of structure and α is the inclination of structure. A block moves smoothly across the surface, and its shape is illustrated in Figure 5. In this model, the *FS* of the block can be calculated by Equation (11) as:

$$FS = \frac{N1tan\emptyset 1 + N2tan\emptyset 2 + c1S1 + c2S2}{GSin\theta} \quad (11)$$

Where, ϕ_1, ϕ_2 and c_1, c_2 are friction and cohesion of the cut slope material, respectively, and θ is the dip of the intersection of the slipping plane S_1 and S_2. In Equation (11) N_1, N_2 is the normal force of the slipping planes and fulfills Equations (12) and (13). Where θ_1 and θ_2 are the angles between the upper normal of the plane.

$$\sin\theta = \frac{z_2 - z_1}{\sqrt{(x_1 - x_2)^2 + (y_1 - y_2)^2 + (z_1 - z_2)^2}} \quad (12)$$

$$N = G\cos\theta \quad N_1 = \frac{G\cos\theta\sin\theta_1}{\sin(\theta_1 + \theta_2)} \quad N_2 = \frac{G\cos\theta\sin\theta_2}{\sin(\theta_1 + \theta_2)} \quad (13)$$

Finally, the factor of safety for each slippery block can be calculated by using Equation (14).

$$f_{si} = \frac{N_1\tan\varphi_1 + N_2\tan\varphi_2 + c_1S_1 + c_2S_2}{G\sin\theta} \quad (14)$$

In Equation (14) f_{si} is the safety factor of the block. ϕ_1, ϕ_2, and c_1, c_2 are friction and cohesion of the cut slope material, respectively, and θ is the dip of the intersection of the slipping plane S_1 and S_2. N_1, N_2 is the normal force of the slipping planes. θ_1 and θ_2 are

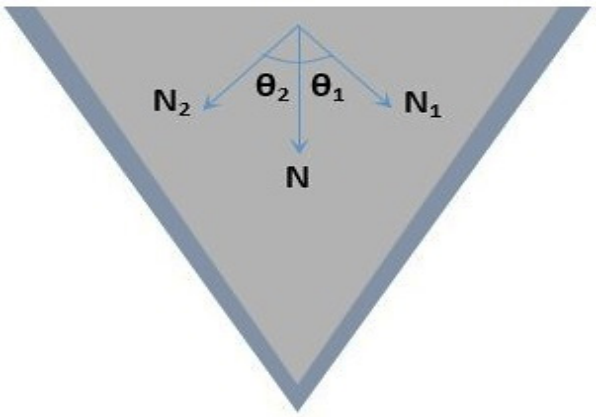

Fig. 5. Double sliding surface model.

the angles between the upper normal of the plane and *G* is the gravity of the block.

4. SLIPPERY BLOCKS CLASSIFICATION

4.1. GeoSMA^{3D} Computer Code

Wang *et al*. [14] developed a 3D numerical slope stability analysis computer program (GeoSMA^{3D}) for identifying rock sliding blocks. This program can simulate a discontinuity network, the number of slippery blocks, its sliding planes, the volume of blocks, and the corresponding *FS* [21]. The flow chart in Figure 6 shows the scheme of analysis and the development of the program.

4.2. Sliding Blocks Stability Simulation

Rock block theory and a three-dimensional numerical slope stability analysis computer program GeoSMA^{3D} are used in the current study to simulate the *FS* of each slippery block. The main analysis procedures include three-dimensional discontinuity network simulation of slope, closed block identification, removable and slippery block identification, *FS* calculation, joint plane simulation, and volume and sliding faces of blocks determination through this software [10, 21, 22].

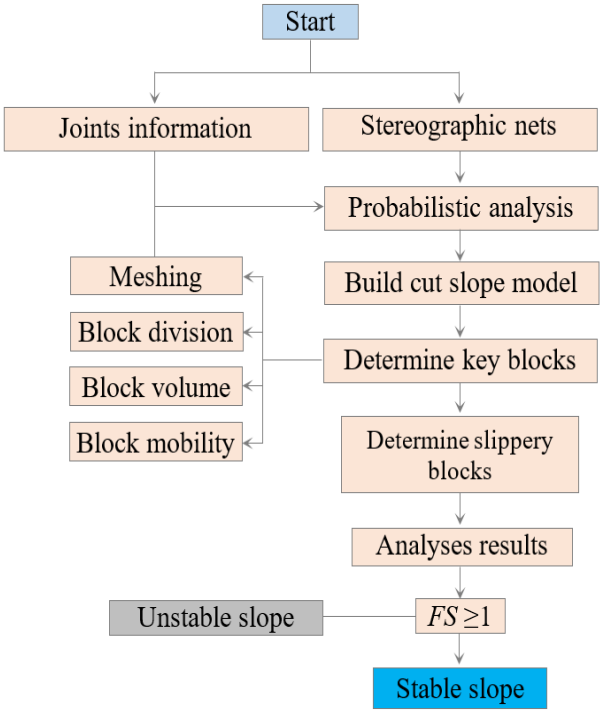

Fig. 6. Flowchart scheme showing the stability analysis procedure in GeoSMA^{3D}, after Wang and Ni [21].

The slope was modeled with a length of 60 m, width of 80 m, height of 40 m, and crest of 20 m in GeoSMA^{3D} software as shown in Figure 7. The dip angle was determined as 60°. Then the value of internal friction angle and cohesion were taken from Table 2.

The method presented by Wang and Ni [21] is selected within the framework of GeoSMA^{3D} to compute the stability of each slippery block and the results are shown in Figure 8. Joints are indicated by the trace lines. The pattern of the slippery blocks yields the shapes of all wedge blocks. Most of the slippery blocks were tetrahedrons or hexahedrons. The distribution, shape, and position of all the slippery blocks of the rock slope. The safety factor, volume of slippery blocks, and the number of sliding faces of each slippery block were determined. The slippery block whose *FS* is smaller than one harms the stability of the whole slope.

5. STABILITY SIMULATION

5.1. Models Parameters and Failure Criterion

According to slope geometry, a possible model is created in 3DEC software (Figure 9). The material strength parameters are assigned according to Table 2. Mohr-Coulomb yield criterion is selected to model the material behavior. The stability of the whole slope is simulated via the shear strength reduction method. In this paper. The rock slope model is divided into hexahedral blocks composed of hexahedrons 4 m in size. Then this slope model is imported into the three-dimensional distinct element code (3DEC) as a numerical model. The number of blocks and apexes in the numerical model were

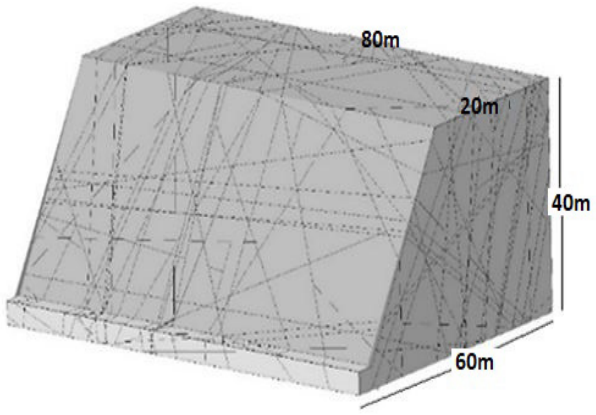

Fig. 7. Slope model with joint planes.

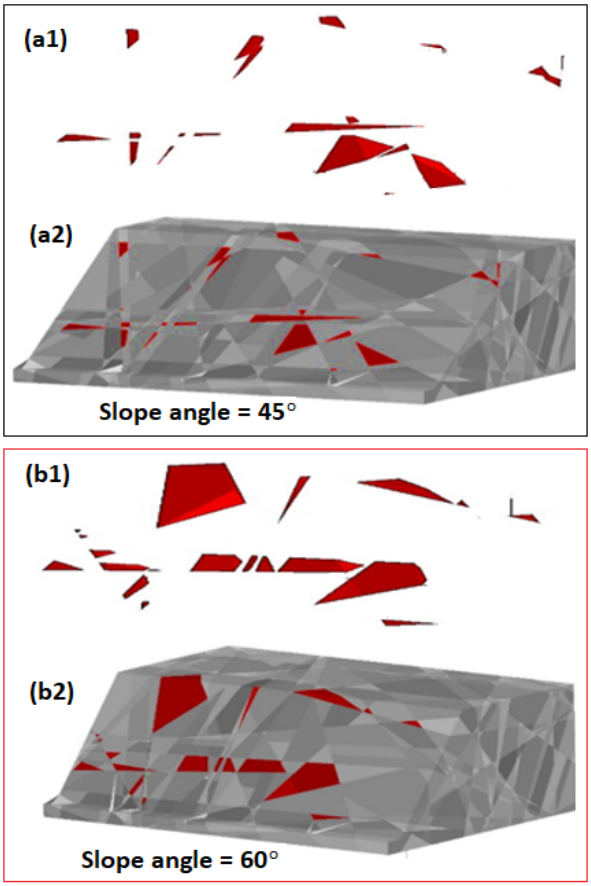

Fig. 8. All Slippery blocks in red color. Shapes of slippery blocks (a1, b1) and location of slippery blocks (a2, b2).

18389 and 112464, respectively. Each hexahedron is assumed as a rigid block in the numerical model. The input properties for the jointed rock slope and discontinuities are presented in Tables 1 and 2. It should be noted that the parameters for the virtual joints formed by the interfaces between blocks need to be carefully determined based on the lithology of the rock mass. In Table 1, γ is the unit weight, c is cohesion, ϕ is the internal friction angle, G is the shear modulus, B is the bulk modulus, k_n is the normal stiffness of the discontinuity, and K_s is shear stiffness of the discontinuity.

3DEC uses the shear-strength reduction method (SRM) to perform the stability analysis of geotechnical structures. Several simulations were executed by increasing the trial value of reduction factor (f) until slope failure. The safety factor (FS), at failure, equals the trial value of f [23]. In the strength reduction technique, the φ and c are reduced at different trial values of SRF until cut slope failure occurs as:

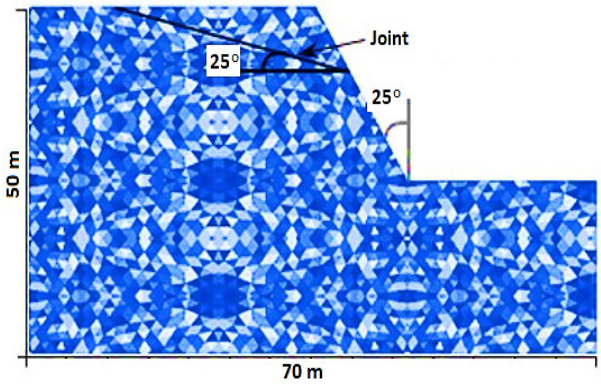

Fig. 9. Geometry of slope and joint position.

$$Cf = c/f \tag{15}$$

$$\varphi f = arctan(\frac{tan\varphi}{f}) \tag{16}$$

Where c_f is reduced cohesion and φ_f reduced internal friction angle.

The failure of the slope has two obvious characteristics in the 3DEC modeling process: (i) there is no slippery block, and most of the blocks on the entire slope are nearly static; although a few blocks are displaced, these blocks are not moved out of the boundary of the model, as shown in Figure 10(a). (ii) A small number of blocks will slip out of the model boundary, which also triggers the movement of some other blocks. Some blocks will become unstable and eventually induce large-scale sliding (Figure 10b).

6. RESULTS AND DISCUSSION

In the current study, rock slope stability was simulated through numerical modeling. Rock block theory within the network of GeoSMA^{3D} software was used to identify slippery blocks and the stability of each slippery block. The relationship between the number of slippery blocks and the corresponding FS of each slippery block was assessed. It has been observed that most of the slippery blocks have a value of FS less than one, and only three blocks have an FS of more than 1.1; these three blocks have distinct key blocks [24]. For that reason, this can be decided that the proper dressing of the rock slope is favorable to improve the stability along the road.

To study the cut slope stability, two different slope angles of 45° and 60° were selected, because

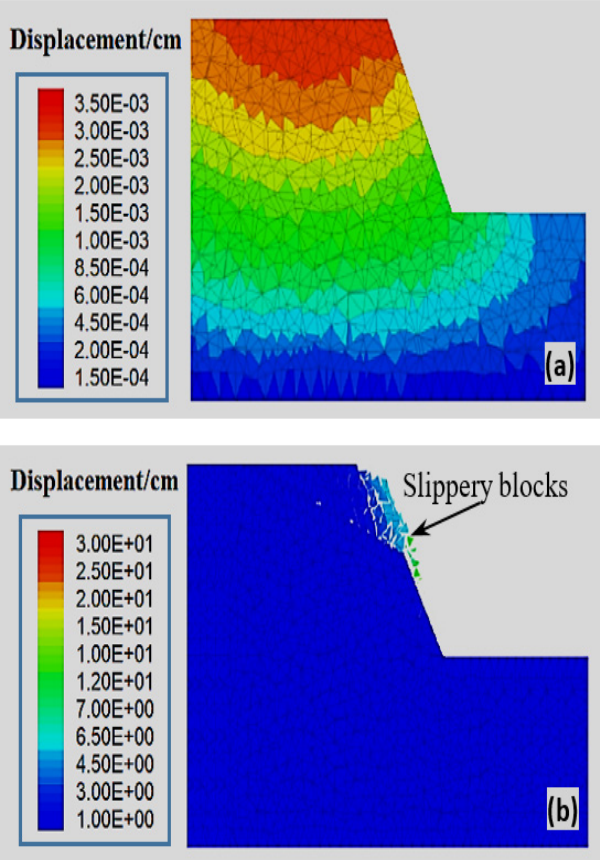

Fig. 10. (a) Zero slippery block, and (b) few slippery blocks.

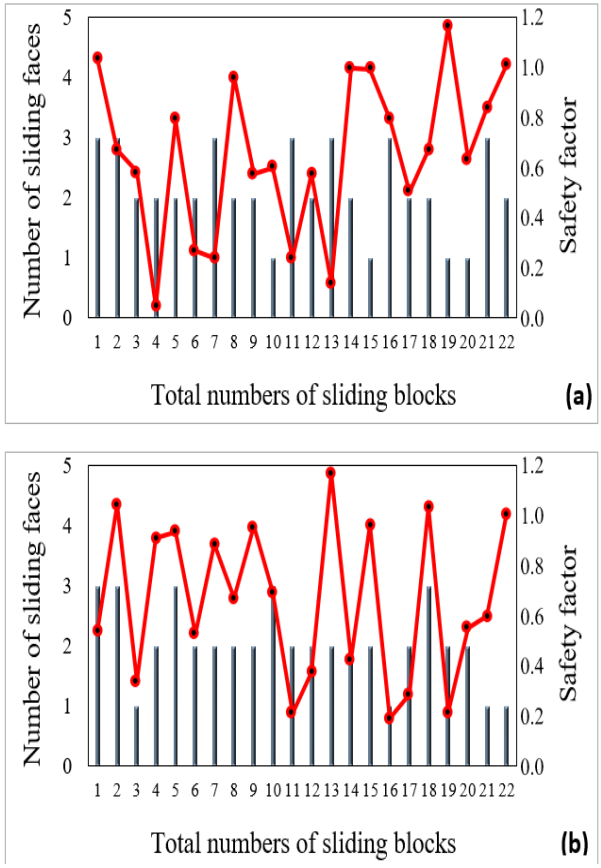

Fig. 11. Relationship diagram between block sliding faces and corresponding *FS*. (a) The slope angle is 45°, and (b) the slope angle is 60°.

the slope angle ranges from 45° to 60°. Figure 11 shows a schematic diagram of the slippery blocks searched at slope angles of 45° and 60°. The volume of block and *FS* was largely affected by the slope angle [25]. The safety factor decreased as the number of block sliding faces increased. This can be seen that as the slope angle becomes larger, the number of slippery blocks maintains a certain range, but the overall sliding surfaces of the block and the volume of each block have increased on a large scale [26]. Meanwhile, the safety factors of block number 1, 19, and 22 are larger than 1.1, when the slope dip is considered as 45° (Figure 11a). In addition, the *FS* of block numbers 2, 13, and 18 are more than 1.1 when the slope dip is considered as 60° (Figure 11b). These blocks could improve the stability and reinforcement measurement quality of rock slopes.

The concentration of shear stress in different zones of slope is examined, as shown in Figure 12. The maximum concentration of shear stress of 5.945×10^3 MPa is observed at the upper part of the

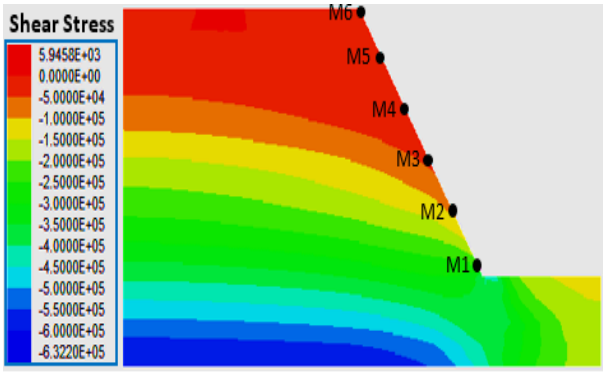

Fig. 12. Contour of shear stress and six various monitoring points.

slope. At the slope toe, the maximum shear stress of -3.00×10^5 is recorded. At six monitoring points, the displacement history of the slope is studied via 3DEC considering two different slope angles and heights. The *x*-displacements were rising in monitoring locations near to slope crest as shown in Figure 13. When the slope angle was 45°, the maximum *x*-displacement of 14 cm at monitoring location M6 was recorded.

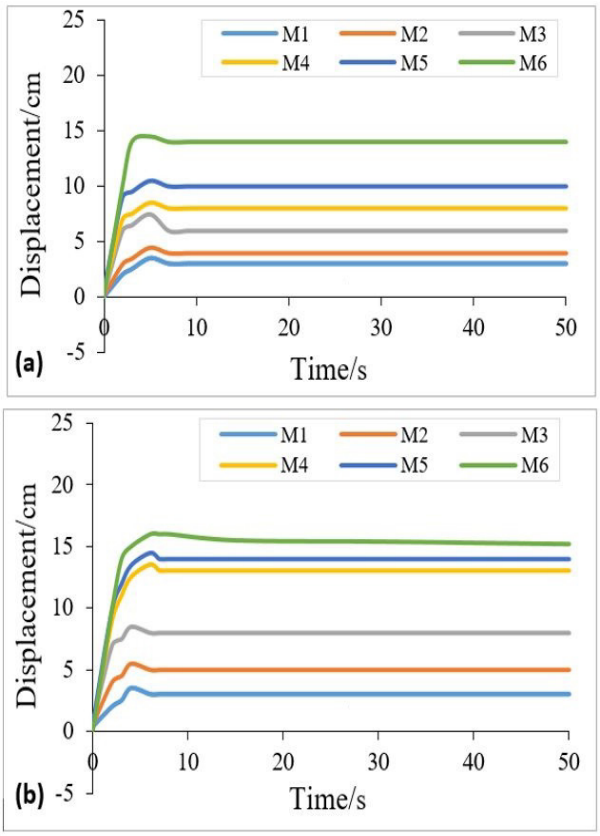

Fig. 13. Displacement history plot at various monitoring points. (a) The slope angle is 45°, and (b) the slope angle is 60°.

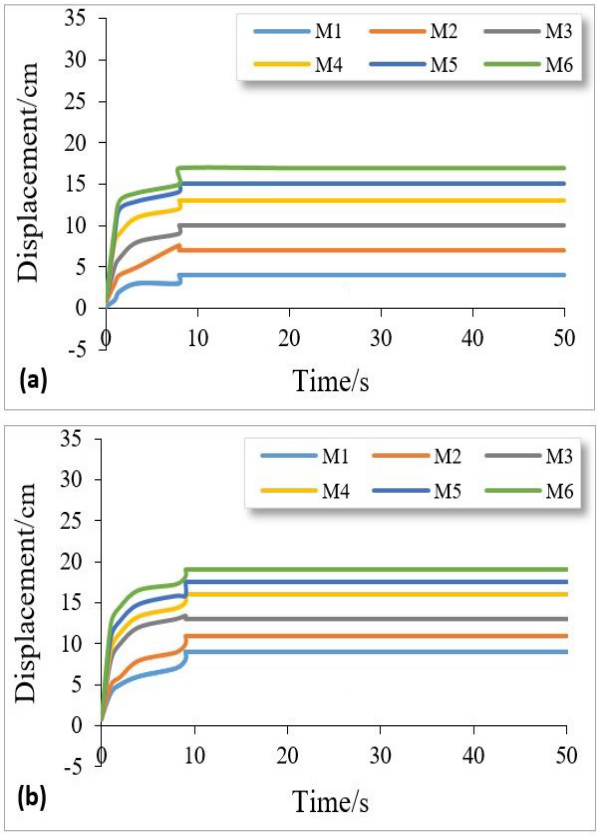

Fig. 14. Displacement history plot at various monitoring points. (a) Slope height is 40 m, and (b) slope height is 60 m.

The maximum *x*-displacement of 16 cm at monitoring location M6 was observed when the slope angle was 60°. It means, that as the slope angle rose the *x*-displacement also rose significantly. This is because of a higher angle, which produces more gravity resulting in a higher value of displacement. At monitoring locations M1, M2, and M3, the *x*-displacement was lower than that of the monitoring locations M4, M5, and M6. The higher value of displacement around the crest can cause big planner failure of the slope. So, the upper part of the slope needs more attention during slope reinforcement design.

Considering different heights of slope, the *x*-displacement history plot is presented in Figure 14. Slope height has a remarkable effect on slope. At slope heights of 40 m and 60 m, the maximum x-displacement of 16.4 cm and 21 cm was recorded, respectively. The horizontal displacement of the slope first suddenly increased at a time of 10, and after that, it maintained the same value. Almost similar observations were noted in all cases. The magnitude of displacement in the first case was higher as compared to the second case. Based on numerical investigations, strain concentration, and displacement history plots indicate that the mud rock slope is most likely to fail by the big planner at the top.

7. CONCLUSIONS

In this research, GeoSMA^{3D} and 3DEC software were used to analyze the stability of rock slope form by mudstone. From the numerical simulations, the following conclusions are drawn:

1. Rock block theory is adopted within the framework of GeoSMA^{3D} software to search key slippery blocks. Block volume, block sliding faces, and corresponding *FS* were determined by the numerical tool. Results suggest that most of the blocks have *FS* less than one.
2. The progressive failure of the cut slope was examined by the strength reduction method within the system of 3DEC. This was computed from the shear strain and displacement contour

plots at different slope angles and heights. Increasing the slope angle and height increase in *x*-displacement is recorded. Numerical outcomes showed that a big planner failure can take place at the upper portion of the slope.

3. Numerical results suggest that slope angle and height are important factors that affect the failure modes of slope. Results also indicate that the slope is unstable. Therefore, it needs to take proper slope reinforcement measures.

This study only considered static loads, so in future research dynamic loads and rainfall intensity must be taken into account for better understanding.

8. ACKNOWLEDGEMENTS

This work was conducted with the support of Mir Chakar Khan Rind University of Technology, DG Khan; Bahauddin Zakariya University, Multan; the National Highway Authority (NHA) of Pakistan; and Fort Munro Development Authority, DG Khan.

9. CONFLICT OF INTEREST

The authors declare no conflict of interest.

10. REFERENCES

1. S. Wang, Z. Ahmed, and P. Wang. Study of critical failure surface influencing factors for loose rock slope. *SN Applied Sciences* 3: 65 (2021).
2. H. Wang, J. Zou, X. Wang, P. Lv, Z. Tan, L. Cheng, W. Qiang, Q. Binli, and G. Zhengchao. Analysis of deformation mechanism of rainfall-induced landslide in the Three Gorges Reservoir Area: Piansongshu landslide. *Scientific Report* 14: 10005 (2024).
3. L.R. Alejano, B. Pons, F.G. Bastante, E. Alonso, and H.W. Stockhausen. Slope geometry design as a means for controlling rockfalls in quarries. *International Journal of Rock Mechanics and Mining Sciences* 44: 903-921 (2007)
4. Y. Zheng, R. Wu, C. Yan, R. Wang, and B. Ma. Numerical study on flexural toppling failure of rock slopes using the finite discrete element method. *Bulletin of Engineering Geology and the Environment* 83: 111 (2024).
5. Z. Chuhan, O. Pekau, J. Feng, and W. Guanglun. Application of distinct element method in dynamic analysis of high rock slopes and blocky structures. *Soil Dynamics and Earthquake Engineering* 16: 385-94 (1997).
6. R. Bhasin and A. Kaynia. Static and dynamic simulation of a 700-m high rock slope in western Norway. *Engineering Geology* 71: 213-26 (2004).
7. L.M. Highland and P. Bobrowsky. The landslide handbook: A guide to understanding landslides. Circular 1325. *US Geological Survey, Reston, Virginia* (2008). https://pubs.usgs.gov/circ/1325/pdf/C1325_508.pdf
8. N. Matsuoka and H. Sakai. Rockfall activity from an alpine cliff during thawing periods. *Geomorphology* 28: 309-328 (1999)
9. V. Solonenko. Landslides and collapses in seismic zones and their prediction. *Bulletin of the International Association of Engineering Geology* 15: 4-8 (1977).
10. S. Wang, Z. Ahmed, M.Z. Hashmi, and W. Pengyu. Cliff face rock slope stability analysis based on unmanned aerial vehicle (UAV) photogrammetry. *Geomechanics and Geophysics for Geo-Energy and Geo-Resources* 5(4): 333-344 (2019).
11. F. Agliardi and G. Crosta. High-resolution three-dimensional numerical modeling of rockfalls. *International Journal of Rock Mechanics and Mining Sciences* 40: 455-471 (2003).
12. S. Vijayakumar, T. Yacoub, and J. Curran. On the effect of rock size and shape in rockfall analyses. *Proceedings of the US Rock Mechanics Symposium (ARMA) San Francisco CA, USA* (2011).
13. D. Varnes. Slope movement types and processes. *Special Report* 176: 11-33 (1978).
14. S. Wang, P. Ni, and M. Guo. Spatial characterization of joint planes and stability analysis of tunnel blocks. *Tunnelling and Underground Space Technology* 38: 357-67 (2013).
15. Y. Liu, H. Li, J. Zhao, J. Li, and Q. Zhou. UDEC simulation for the dynamic response of a rock slope subject to explosions. *International Journal of Rock Mechanics and Mining Sciences* 41: 474 (2004).
16. S. Sarkar, K. Pandit, N. Dahiya, and P. Chandna. Quantified landslide hazard assessment based on finite element slope stability analysis for Uttarkashi–Gangnani Highway in Indian Himalayas. *Natural Hazards* 106: 1895-1914 (2021).
17. P. Singh, A. Wasnik, A. Kainthola, M. Sazid, and T. Singh. The stability of road cut cliff face along SH-121: a case study. *Natural Hazards* 68: 497-507 (2013).
18. L. Zhao, C. Jin, B. Zhao, D. Huang, Z. Zhu, and S. Zuo. A method for setting up passive protective nets for rockfalls based on unmanned aerial vehicle (UAV) photogrammetry. *Bulletin of Engineering Geology and the Environment* 83: 340 (2024).

19. H. Kou, Z. Shi, C. Xia C, Y. Zhou, and S. Meng. Dynamic simulation and failure analysis of intermittently jointed rock cells and slopes based on a novel spring-based smoothed particle hydrodynamics method. *Bulletin of Engineering Geology and the Environment* 83: 135 (2024).
20. B. Gautam and S. Mehndiratta. Analysis of a rock slope with an infilled planar joint using deterministic and probabilistic approaches. *Indian Geotechnical Journal* inpress (2024). https://link.springer.com/article/10.1007/s40098-024-00925-6
21. S. Wang and P. Ni. Application of block theory modeling on spatial block topological identification to rock slope stability analysis. *International Journal of Computational Methods* 11: 1350044 (2014).
22. F. Wang, S. Wang, M.Z. Hashmi, and Z. Xiu. The characterization of rock slope stability using key blocks within the framework of GeoSMA-3D. *Bulletin of Engineering Geology and the Environment* 77: 1405-1420 (2018).
23. J. Xiao, W. Gong, J.R. Martin, M. Shen, and Z. Luo. Probabilistic seismic stability analysis of slope at a given site in a specified exposure time. *Engineering Geology* 212: 53-62 (2016).
24. S. Wang, Z. Zhang, C. Wang, C. Zhu, and Y. Ren. Multistep rocky slope stability analysis based on unmanned aerial vehicle photogrammetry. *Environmental Earth Sciences* 78: 260 (2019).
25. Q.H. Zhang and G.H. Shi. Discussion on Key Issues in the Application of Block Theory in Rock Engineering. *Rock Mechanics and Rock Engineering* 57: 2017-2033 (2024).
26. S. Dong, Q. Zhang, Z. Mai, and H. Zhang. A Limit Equilibrium Method for Analyzing Multi-sliding-Plane Block Stability and Its Application in the Optimal Design of a Gravity Dam Foundation. *Rock Mechanics and Rock Engineering* 57: 4107-4128 (2024).